JOURNAL OF SOLID STATE CHEMISTRY 108, 371–380 (1994)

The Synthesis, Structure, and Characterization of a Novel 24-Layer Oxide: $Ba_8V_7O_{22}$ with V(III), V(IV), and V(V)

Guo Liu and J. E. Greedan[1]

Institute for Materials Research, McMaster University, Hamilton, Ontario L8S 4M1, Canada

Received March 26, 1993; accepted June 9, 1993

$Ba_8V_7O_{22}$, the first vanadium oxide in which both VO_4^{4-} and VO_6^{8-} coordinations and the coexistence and ordering of all the three common oxidation states of vanadium (+3, +4, and +5) are observed, has been synthesized by reducing $Ba_2V_2O_7$ in hydrogen at 1350°C. Single crystals of $Ba_8V_7O_{22}$ have been grown by rapid cooling of its melt from ~1530°C. Its crystal structure has been solved by single crystal X-ray diffraction, and magnetic and electrical properties have been examined. $Ba_8V_7O_{22}$ crystallizes in the trigonal system, space group $R\bar{3}m$ (No. 166), with hexagonal lattice parameters a = 5.7841(7) Å, c = 57.074(11) Å, V = 1653.6(8) Å^3, and Z = 3. The structure consists of face-shared VO_6^{8-} and VO_6^{9-} octahedra that form $V_3O_{12}^{14-}$ trimers, corner-shared VO_4^{4-} tetrahedra that are connected to the trimers such that they together form pseudo-two-dimensional magnetic layers perpendicular to the c-axis, and isolated VO_4^{3-} tetrahedra that are arranged in planes separating the magnetic layers. It can also be described in terms of stacking of hexagonally close-packed Ba/O layers along the c-axis as a 24-layer structure with the stacking sequence of $(hcc'hhc'ch)_3$, where h and c are hexagonal and cubic BaO_3 layers, respectively, and c' is a cubic BaO_2 layer. Vanadium atoms occupy the tetrahedral sites and $\frac{3}{4}$ of the octahedral sites in an ordered fashion. The 12-layer structure with $(cchh)_3$ stacking, previously proposed for $BaFeO_{3-x}$ but improperly described in space group $R3m$, is redescribed in $R\bar{3}m$. The 24R structure of $Ba_8V_7O_{22}$ is closely related to the 12R structure. $Ba_8V_7O_{22}$ is a semiconductor with three activation energies ranging from 0.31 to 0.48 eV in the temperature range investigated (145–295 K), and a room temperature resistivity of about 12 Ω · cm. Its magnetic behavior is very complicated. Single crystal samples show a broad susceptibility maximum at 280 K, followed by an increasing susceptibility at lower temperatures and additional anomalies at 50 and 20 K.

INTRODUCTION

Tetravalent vanadium is known to form large numbers of oxides with square pyramidal and octahedral coordinations. Tetrahedral coordination for V(IV) is rare. A recent example of a well-characterized oxide containing VO_4^{4-} is the metastable high-temperature form of Sr_2VO_4 (1). Ba_3VO_5 (2) and Ba_2VO_4 (3) are the only other VO_4^{4-}-containing compounds for which structural data are available. Claims have long been made (4, 5) that a $BaVO_3$ phase, whose powder X-ray diffraction pattern is nearly identical to that of $Ba_3V_2O_8$ except for a few additional weak reflections, contains VO_4^{4-}, but its structure remains unknown. Nonetheless, existing examples tend to suggest that large counter cations, such as Ba^{2+}, favor tetrahedral coordination for V(IV). Thus we became interested in the $BaVO_3$ system as part of an effort to understand the crystal chemistry and physical properties of VO_4^{4-}-containing oxides. We have discovered two new structures: the 5-layer $BaVO_{3-x}$ series (x = 0.2, 0.1, 0.0) and the 24-layer $Ba_8V_7O_{22}$. The results for the latter compound are presented here.

EXPERIMENTAL

Sample Preparation

Synthesis of $Ba_8V_7O_{22}$. $Ba_2V_2O_7$ was first synthesized by firing an intimate mixture of $2BaCO_3$ (Aesar, 99.9%) and V_2O_5 (Cerac, 99.9%) at 900–1000°C in air. Powder specimens of $Ba_2V_2O_7$ were reduced in flowing H_2 gas at 1100°C for 24 hr. The black gray product was ground further, pelleted, and confined in an open Mo tube (o.d. 1.25 cm) which was secured in an alumina boat, and heated in preparation grade H_2 gas at 1350°C for 2–4 days depending on the sample size (typically 2–6 g), and cooled down rapidly. The pellet surface near both ends of the Mo tube was partially reoxidized (white) probably during cooling, and the white material was removed physically.

Crystal growth of $Ba_8V_7O_{22}$. First the melting point of $Ba_8V_7O_{22}$ was determined to be about 1450(±50)°C by observing the melting process of a pellet contained in an open Mo crucible while it was gradually heated in a radio frequency induction furnace under a 10^{-4} Torr pressure. The temperature was measured using an optical pyrometer. In the next step pelleted specimens were evacuated first and then sealed into a Mo tube under 0.5 atmosphere argon by arc welding, heated to ~1530°C, soaked for 5

[1] To whom correspondence should be addressed.

0022-4596/94 $6.00

min, then cooled to 1300°C at a rate of ~100°C/hr, and finally cooled rapidly to room temperature. The product was crushed slightly and washed in an ultrasonic cleanser with distilled water for 30 min. Irregularly shaped black crystals were obtained.

Powder X-Ray and Electron Diffraction

Polycrystalline specimens were examined using a Guinier-Hägg camera (IRDAB XDC700) with Cu$K\alpha$1 radiation and a Si standard. The Guinier data were read with a computer-controlled automated LS-20 type line scanner (KEJ Instruments, Täby, Sweden). Electron diffraction patterns were taken in a Philips CM12 transmission electron microscope using crushed polycrystalline specimens supported on holey carbon films.

Single Crystal X-Ray Structure Analysis of $Ba_8V_7O_{22}$

A black crystal was mounted on the tip of a glass fiber using epoxy cement. Data suitable for structure analysis were collected on a Siemens P3 four-circle diffractometer with Ag$K\alpha$ radiation. Data reduction, structural solution, and refinement were effected using the SHELXTL PC software on an 80486 personal computer. The initial unit cell parameters and orientation matrix were determined from a least-squares fit of 24 reflections. Ten azimuthal scans ((1 2 −10); (2 1 −14); (2 2 −24); (2 3 −28); (4 2 −28); (3 4 −28); (3 5 −14); (3 5 −38); (4 5 −28); (4 6 −14)) were used for absorption corrections using the program XEMP based on an ellipsoid model. Possible space groups were found to be $R\bar{3}$, $R3$, $R3m$, $R32$, and $R\bar{3}m$ from the systematic extinction (observed *hkil*: $-h + k + l = 3n$). Intensity statistics suggested that the most likely space group was the centrosymmetric $R\bar{3}m$ (No. 166). Positional parameters of all the heavy atoms (Ba and V) were found by direct methods, and the oxygens were located by difference Fourier. On the basis of intensity statistics and the final successful refinement of the structure, the space group was determined to be $R\bar{3}m$. The positional and anisotropic thermal parameters were refined by full-matrix least-squares methods to $R = 2.32\%$, $R_w = 2.46\%$ and GOF = 1.14 using observed reflections with $F_o^2 > 3\sigma(F_o^2)$. Detailed crystallographic data are listed in Table 1.

Magnetic Susceptibility and Electrical Resistivity Measurements

Susceptibility data were obtained using a Quantum Design SQUID magnetometer in the temperature range 5 to 300 K using pelleted specimens and randomly oriented crystals at an applied magnetic field of 0.2 T. Diamagnetic corrections were applied. Resistivities from 145 to 295 K were measured on a sintered pellet directly from the hydrogen reduction using the standard four-probe method. Contacts were attached to the specimen with silver paste.

Thermogravimetrical Analysis (TGA)

The thermogravimetrical analysis was performed with a Netzsch STA 409 thermal analyzer in flowing O_2 atmosphere at a heating rate of 5°C/min to 800°C. This gave a chemical composition of $BaVO_{2.97\pm0.01}$ for the polycrystalline product. It is believed that very little vanadium was lost during the hydrogen reduction based on the fact that the TGA oxidation product was the phase-pure $Ba_2V_2O_7$ as identified by Guinier X-ray diffraction.

RESULTS AND DISCUSSION

1. Crystal Structures

The Crystal Structure of $Ba_8V_7O_{22}$

Atomic coordinates and isotropic temperature factors are listed in Table 2, anisotropic temperature factors in Table 3, and important bond lengths and bond angles in Table 4. The crystal structure of $Ba_8V_7O_{22}$ is shown in Fig. 1. Several features about this structure are worth noting. First, there exist two types of coordinations for vanadium: VO_6 (V(1) and V(4)) octahedra and VO_4 (V(2) and V(3)) tetrahedra. Next, the VO_6 octahedra form linear V_3O_{12} trimers through face-sharing. Finally, half of the VO_4 ($V(2)O_4$) tetrahedra are isolated, and the other half ($V(3)O_4$) share corners with the trimers. Part of the corner-sharing and face-sharing features is shown in Fig. 2. It is worth emphasizing that units like the one shown in Fig. 2 are not isolated. The corner-sharing extends in planes perpendicular to the *c*-axis.

A close examination of the various V/O polyhedra reveals the existence and ordering of vanadium ions in three different oxidation states in $Ba_8V_7O_{22}$. As can be seen in Table 4, there exist four types of independent VO_4 tetrahedra and VO_6 octahedra, each of which has a distinctly different average V–O bond length. Using the ionic radii compiled by Shannon (6) the V–O bond length is estimated to be 2.02 Å for a VO_6^{9-}, 1.96 Å for VO_6^{8-}, 1.735 Å for a VO_4^{3-}, and 1.79–1.80 Å for a VO_4^{4-} (based on the ionic radii of 4-coordinated Cr^{4+} and Ti^{4+}). Thus our observed data strongly suggest that V(1) is V^{3+}, V(2) V^{5+}, and only V(3) and V(4) can be considered as V^{4+}. The observed values are also consistent with literature data for the respective types of V–O bonds. For example, the average V–O of 2.024(3) Å for $V(1)O_6$ is only slightly longer than that (1.99 Å, VO_6^{9-}) in $LaSrVO_4$ (7); the value of 1.942(1) Å for $V(4)O_6$ is the same as that (1.94 Å, VO_6^{8-}) in Sr_2VO_4 (8); the 1.714(2) Å for $V(2)O_4$ is well within the range of 1.713(5) to 1.719(5) Å found for VO_4^{3-} in $Ba_3V_4O_{13}$ (9); the 1.778(3) Å for $V(3)O_4$ is close to that (1.76(3) Å) for VO_4^{4-} in β-Ba_2VO_4 and β-Sr_2VO_4 (3).

TABLE 1
Summary of Crystallographic Data for $Ba_8V_7O_{22}$

Color; habit	Black; irregular
Crystal size (mm^3)	0.15 × 0.14 × 0.072
Diffractometer	Siemens P3
Radiation	Ag$K\alpha$ (λ = 0.56086 Å)
Temperature (K)	290
Monochromator	Graphite
2θ range (°)	1.5 to 60.0
Index ranges	$0 \le h \le 9$, $-10 \le k \le 8$, $-102 \le l \le 102$
Scan type	ω
Scan speed (°/min)	Variable, 2.00 to 29.30 in ω
Scan range (ω, °)	0.06
Absorption correction	Semiempirical
Min/max transmission	0.235/0.378
Crystal system	Rhombohedral
Space group	$R\bar{3}m$
Unit cell dimensions (Å)	a = 5.7841(7)
	c = 57.074(1)
Volume (Å^3)	1653.6(8)
Z	3
Formula weight	1807.2
Density (calc, g/cm^3)	5.444
Absorption coefficient (mm^{-1})	16.929
F(000)	2355
No. of reflections collected	6869
No. of independent reflections	1351 (R_{int} = 4.10%)
No. of observed reflections	1079 ($F_o^2 > 3\sigma(F_o^2)$)
No. of parameters refined	48
Data/parameter ratio	22.5
R (%)	2.32
R_w (%)	2.46
Goodness-of-fit	1.14
Largest shift/error, Δ/σ	0.001

TABLE 2
Atomic Coordinates and Equivalent Isotropic Displacement Coefficients (Å^2 × 10^3) for $Ba_8V_7O_{22}$

Atom	Site	x	y	z	U (eq)
Ba(1)	6(c)	0	0	0.3172(1)	10(1)
Ba(2)	6(c)	0	0	0.1047(1)	17(1)
Ba(3)	6(c)	0	0	0.1812(1)	10(1)
Ba(4)	6(c)	0	0	0.3891(1)	8(1)
V(1)	6(c)	0	0	0.0435(1)	7(1)
V(2)	6(c)	0	0	0.4653(1)	9(1)
V(3)	6(c)	0	0	0.2565(1)	7(1)
V(4)	3(a)	0	0	0	8(1)
O(1)	18(h)	0.1527(2)	$-x$	0.0210(1)	10(1)
O(2)	18(h)	0.1714(2)	$-x$	0.1420(1)	15(1)
O(3)	18(h)	−0.1675(2)	$-x$	0.0641(1)	12(1)
O(4)	6(c)	0	0	0.2272(1)	40(2)
O(5)	6(c)	0	0	0.4356(1)	31(2)

Note. Equivalent isotropic U defined as one third of the trace of the orthogonalized U_{ij} tensor

TABLE 3
Anisotropic Displacement Coefficients (Å^2 × 10^3) for $Ba_8V_7O_{22}$

Atom	$U_{11} = U_{22}$	U_{33}	U_{12}	U_{13}	U_{23}
Ba(1)	9(1)	10(1)	$\frac{1}{2}U_{11}$	0	0
Ba(2)	22(1)	8(1)	$\frac{1}{2}U_{11}$	0	0
Ba(3)	11(1)	9(1)	$\frac{1}{2}U_{11}$	0	0
Ba(4)	9(1)	8(1)	$\frac{1}{2}U_{11}$	0	0
V(1)	7(1)	7(1)	$\frac{1}{2}U_{11}$	0	0
V(2)	10(1)	8(1)	$\frac{1}{2}U_{11}$	0	0
V(3)	8(1)	6(1)	$\frac{1}{2}U_{11}$	0	0
V(4)	7(1)	11(1)	$\frac{1}{2}U_{11}$	0	0
O(1)	12(1)	9(1)	8(1)	0(1)	$-U_{13}$
O(2)	16(1)	16(1)	11(1)	0(1)	$-U_{13}$
O(3)	12(1)	15(1)	7(1)	2(1)	$-U_{13}$
O(4)	52(3)	16(3)	$\frac{1}{2}U_{11}$	0	0
O(5)	42(2)	8(2)	$\frac{1}{2}U_{11}$	0	0

Note. The anisotropic displacement exponent takes the form: $-2\pi^2(h^2a^{*2}U_{11} + \ldots + 2hka^*b^*U_{12})$

TABLE 4
Important Bond Lengths (Å) and Bond Angles (°) for $Ba_8V_7O_{22}$

	$Ba(1)O_{12}$			$Ba(2)O_{12}$	
Ba(1)–O(1)	(×3)	2.784(2)	Ba(2)–O(3)	(×3)	2.861(2)
Ba(1)–O(1)′	(×6)	2.909(1)	Ba(2)–O(5)	(×3)	3.342(1)
Ba(1)–O(3)	(×3)	3.205(3)	Ba(2)–O(4)	(×3)	3.340(1)
Average		2.952(2)	Ba(2)–O(2)	(×3)	2.734(2)
			Average		3.069(2)
	$Ba(3)O_{10}$			$Ba(4)O_{10}$	
Ba(3)–O(4)		2.628(6)	Ba(4)–O(1)	(×3)	2.685(2)
Ba(3)–O(2)	(×3)	2.820(2)	Ba(4)–O(3)	(×6)	2.931(1)
Ba(3)–O(2)′	(×4)	2.950(2)	Ba(4)–O(5)		2.657(5)
Ba(3)–O(2)″	(×2)	2.950(1)	Average		2.830(2)
Average		2.879(2)			
	$V(1)O_6$			$V(2)O_4$	
V(1)–O(1)	(×3)	1.998(2)	V(2)–O(2)	(×3)	1.720(1)
V(1)–O(3)	(×3)	2.050(3)	V(2)–O(5)		1.695(5)
Average		2.024(3)	Average		1.714(2)
O(3)–V(1)–O(1)	(×6)	93.2(1)	O(2)–V(2)–O(2)′	(×3)	109.5(1)
O(3)–V(1)–O(1)′	(×3)	175.0(1)	O(2)–V(2)–O(5)	(×3)	109.4(1)
O(1)′–V(1)–O(1)″	(×3)	83.1(1)			
O(3)–V(1)–O(3)	(×3)	90.3(1)			
	$V(3)O_4$			$V(4)O_6$	
V(3)–O(4)		1.669(6)	V(4)–O(1)	(×2)	1.942(1)
V(3)–O(3)	(×2)	1.814(2)	V(4)–O(1)′	(×4)	1.942(2)
V(3)–O(3)′		1.813(3)	Average		1.942(1)
Average		1.778(3)			
O(4)–V(3)–O(3)	(×3)	113.6(1)	O(1)–V(4)–O(1)′	(×3)	180.0(1)
O(3)–V(3)–O(3)′	(×3)	105.0(1)	O(1)–V(4)–O(1)″	(×6)	86.0(1)
			O(1)′–V(4)–O(1)″	(×6)	94.0(1)
		V···V and shortest O···O distances			
V(1)···V(4)		2.482(1)	V(1)···V(3)		3.844(2)
V(2)···V(2)′		3.959(2)	O(1)···O(1)′		2.650(2)

According to Brown and Altermatt (10) the bond valence sum (BVS) for a given ion is expected to be close to the oxidation state of the ion, normally. Bond valence sums for the crystallographically independent atoms are thus calculated using the observed bond lengths and listed in Table 5. It is clear that the same valence assignments for the vanadium atoms as above are suggested by their bond valence sums.

Based on the above valence analysis, the chemical formula can then be written as $Ba_8V_3^{4+}V_2^{3+}V_2^{5+}O_{22}$. This is a remarkably rare compound in which all three common oxidation states of the transition metal coexist, and to our knowledge it is the first vanadium oxide in which both VO_6^{8-} octahedra and VO_4^{4-} tetrahedra are observed. The face-sharing of VO_6 octahedra, on the other hand, is a common feature found in many $BaMO_3$-typed layered oxides of transition metals (M).

Powder X-Ray and Electron Diffraction of $Ba_8V_7O_{22}$

The black polycrystalline material prepared from hydrogen reduction of $Ba_2V_2O_7$ was well crystallized and exhibited sharp reflection lines. Early investigations showed that its powder X-ray diffraction pattern was somewhat similar to that of the 12-layer $BaFeO_{3-x}$ ($x \approx 0.10$) (11), but more reflections were observed for the former. All but three very weak reflections can be accounted for based on the rhombohedral symmetry of Ba FeO_{3-x} with least-squares refined hexagonal cell parameters $a = 5.7789(4)$ Å, $c = 28.522(3)$ Å. The 12-layer structure model for $BaFeO_{2.93}$ (12) was then tested for profile refinements using both powder neutron and X-ray diffraction data. No satisfactory results were obtained.

It was later found by electron diffraction that the c-axis was actually twice that of the 12-layer structure. The electron diffraction pattern along the [0 1 0] zone axis and the electron microscopic image of a crystal are both shown in Fig. 3. The specimens examined were well crystallized. The diffraction pattern clearly revealed the rhombohedral symmetry. Only (hkl) reflections with $-h + k + l = 3n$ were observed. From this pattern the hexagonal cell parameters were estimated to be $a \approx 5.76$ Å and $c \approx 57.3$ Å. Therefore, the structure should be 24-layered. All the

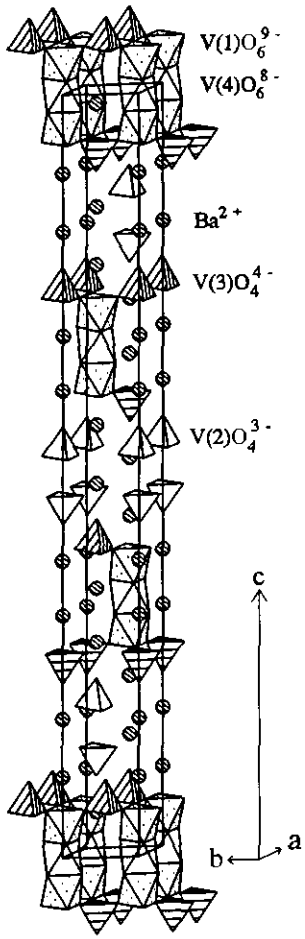

FIG. 1. The crystal structure of $Ba_8V_7O_{22}$ showing the isolated and corner-shared VO_4 tetrahedra and face-shared VO_6 octahedra.

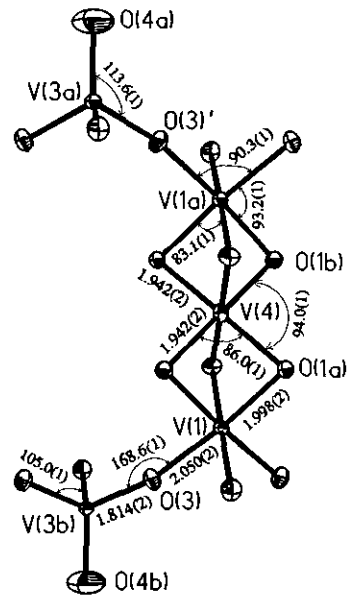

FIG. 2. Connections of face-shared $V(4)O_6^{8-}$ and $V(1)O_8^{9-}$ octahedra in a $V_3O_{12}^{14-}$ trimer and between the trimer and corner-shared $V(3)O_4^{4-}$ tetrahedra. Atoms are plotted at 90% probability level.

observed powder reflections can then be indexed based on the 24-layer model with $a = 5.7791(4)$ Å and $c = 57.045(5)$ Å, $V = 1649.9(2)$ Å^3, which were obtained by a least-squares refinement of 28 unique reflections. The Guinier powder reflections are listed in Table 6.

The single crystal X-ray diffraction results have proved unequivocally the 24*R* structure. The lattice parameters of the crystals, $a = 5.7841(7)$ Å and $c = 57.074(11)$ Å, $V = 1653.6(4)$ Å^3, matched very well with those from the powder X-ray diffraction data. Thus it is believed that the same phase in polycrystalline form has essentially the same chemical composition and structure as the single crystals.

The composition $Ba_8V_7O_{22}$ suggests that polycrystalline specimens prepared from $Ba_2V_2O_7$ must include a vanadium-containing impurity phase to balance the mass of vanadium since it has been shown in the TGA experiment that very little vanadium, if any, was lost under the preparation conditions. In fact, the 5*H* $BaVO_{2.80}$ was obtained when this product was reduced further. However, careful examinations of the Guinier X-ray diffraction patterns revealed no additional reflections that do not belong to the $Ba_8V_7O_{22}$ phase. Thus the impurity level in the polycrystals was probably too low to be observed by X-ray diffraction. On the other hand, the bulk crystals contained about 5–10% $Ba_3V_2O_8$ which forms easily at high temperatures in a Ba–V–O system. Unfortunately, all attempts to synthesize pure $Ba_8V_7O_{22}$ have been unsuccessful. When stoichiometric precursors such as a mixture of $16Ba_3V_2O_8$ and $5V_2O_3$ or $5Ba_2V_2O_7$ and $2Ba_3V_2O_8$ were reduced by hydrogen under the same conditions as described in the Experimental section, the product was always dominated by $BaVO_{2.80}$ which was contaminated by a small amount of Ba_2VO_4 (probably a mixture of $6BaVO_{2.80}$ and Ba_2VO_4).

Stacking Sequences of 24R $Ba_8V_7O_{22}$ and 12R $BaFeO_{3-x}$

The $Ba_8V_7O_{22}$ structure can be described alternatively in terms of stacking of hexagonally close-packed Ba/O

TABLE 5
Bond Valence Sums (BVS) for the Crystallographically Independent Atoms in $Ba_8V_7O_{22}$

Atom	Ba(1)	Ba(2)	Ba(3)	Ba(4)	
BVS	2.14	1.87	2.10	2.43	
Atom	V(1)	V(2)	V(3)	V(4)	
BVS	2.81	5.09	4.13	3.91	
Atom	O(1)	O(2)	O(3)	O(4)	O(5)
BVS	−2.12	−2.12	−2.00	−1.93	−1.81

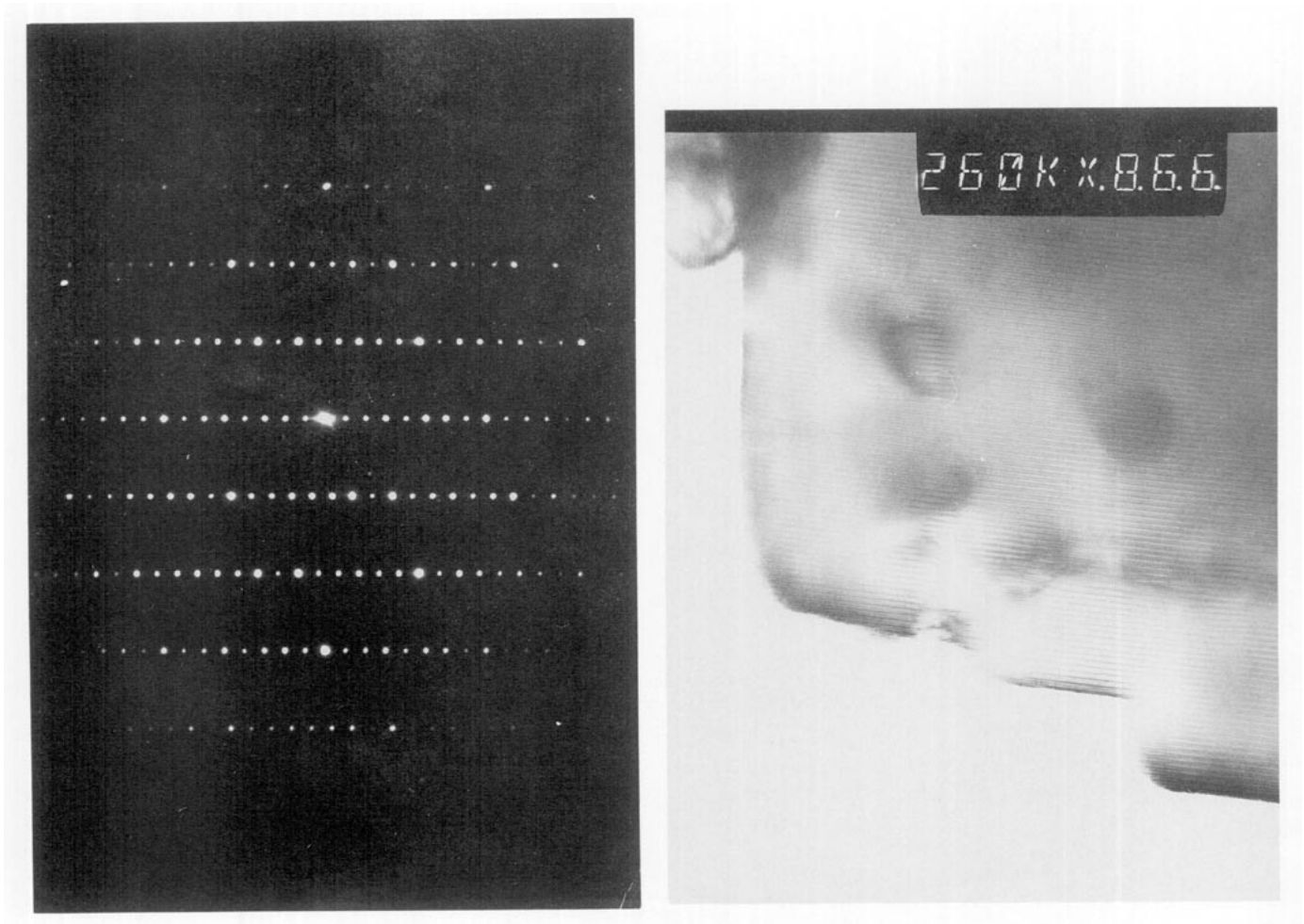

FIG. 3. Electron diffraction pattern of a $Ba_8V_7O_{22}$ crystal in the polycrystalline specimens along the [0 1 0] zone axis (left) and its electron microscopic image (right).

layers and the occupation of tetrahedral and octahedral sites by V atoms as shown in Fig. 4c. It consists of 24 layers of Ba/O stacked along the c-axis in the sequence of $(hhcc'hhc'c)_3$, or $(hcc'hhc'ch)_3$ to emphasize its center of symmetry, where h and c are hexagonal and cubic BaO_3 layers, respectively, and c' is a cubic BaO_2 layer (still termed as cubic because of its Ba position). Typical BaO_3 and BaO_2 layers are depicted in Figs 5a and 5b, respectively. Though both are hexagonally close-packed, the BaO_2 (c') layer is apparently less densely packed than the BaO_3 to retain the same dimension. Vanadium atoms occupy all the (two) tetrahedral O_4 sites and $\frac{3}{4}$ of the octahedral O_6 sites as will be described below in more detail.

The exact doubling of the c-axis of the 24-layer structure with respect to the 12R structure, and the similarity of the stacking sequence $(hhcc'hhc'c)_3$ of $Ba_8V_7O_{22}$ to that of the latter, $(hhcc)_3$, suggest that there is probably a link between these two structures. In order to understand their relationship, it is necessary to examine the 12R structure in detail as well.

The stacking sequence and the resulting basic structure of 12R was described previously (11), and a reasonably good profile refinement based on this model has been performed recently for $BaFeO_{2.93}$ (*12*) using powder X-ray diffraction data. However, there was an error in the choice of origin for the unit cell when this model was first proposed (11), and the error was not corrected in the subsequent profile refinement (12). The given positional parameters (11) are inconsistent with the centrosymmetric space group $R\bar{3}m$ as originally intended. Instead, they are valid only for the noncentrosymmetric polar space group, $R3m$, in which the origin can be chosen arbitrarily. In fact, Parras *et al.* (12) could not refine the $BaFeO_{2.93}$ structure in $R\bar{3}m$ properly using this 12R model; it inevitably gave an extremely short Ba $\cdots$ Fe distance (0.96 Å), and they resorted to $R3m$.

However, the stacking sequence $(hhcc)_3$ can be centro-

TABLE 6
Observed Guinier Powder X-Ray Diffraction Pattern of $Ba_8V_7O_{22}$

h	k	l	d_{cal}	d_{obs}	I_{obs}
0	0	3	19.0150	—	—
0	0	6	9.5075	9.70	2
1	0	4	4.7224	4.719	3
1	0	10	3.7621	3.761	9
0	1	14	3.1598	3.1590	78
1	1	0	2.8895	2.8898	100
1	0	19	2.5746	2.5733	2
0	2	4	2.4648	2.4666	3
0	0	24	2.3769	2.3763	7
2	0	8	2.3612	2.3633	4
0	2	10	2.2916	2.2915	12
0	1	23	2.2223	2.2211	2
2	0	14	2.1324	2.1328	41
0	2	16	2.0482	2.0481	5
1	0	28	1.8870	1.8867	12
1	1	24	1.8356	1.8355	4
1	2	14	1.7159	1.7157	27
3	0	0	1.6683	1.6682	18
1	1	30	1.5884	1.5887	2
0	2	28	1.5799	1.5800	7
2	2	0	1.4448	1.4447	23
2	2	3	1.4406	1.4395	3
2	1	28	1.3862	1.3862	11
3	1	14	1.3139	1.3139	11
1	1	39	1.3050	1.3055	2
0	1	44	1.2550	1.2551	1
2	2	24	1.2346	1.2346	4
1	1	42	1.2292	1.2293	3
0	4	14	1.1961	1.1959	5
1	2	38	1.1759	1.1757	2
1	3	28	1.1471	1.1471	6

Note. Space group $R\bar{3}m$, a = 5.7791(4) Å, c = 57.045(5) Å, V = 1649.9(2) Å^3, Z = 3.

symmetric as can be seen easily from the rearranged sequence $(hcch)_3$ or $(chhc)_3$. To reflect the symmetry center, we introduce a new unit cell for the ideal 12R structure as depicted in Fig. 4a. It can be obtained simply by shifting the origin of the unit cell proposed by Zanne and Gleitzer (11) by $(0, 0, \frac{1}{24})$. The basic structure remains unchanged. Positional parameters derived from the new unit cell for an ideal 12R structure are listed in Table 7. Interestingly, after the same origin shift is applied to the positional parameters of the refined structure of $BaFeO_{2.93}$, the atoms are seen to be correlated strongly by a symmetry center (Table 7). Therefore, the profile refinement results of $BaFeO_{2.93}$ actually tend to support the $R\bar{3}m$ space group proposed here.

Structural Relationship of 24R $Ba_8V_7O_{22}$ with 12R $BaFeO_{3-x}$

To relate the structure of 24R $Ba_8V_7O_{22}$ to the 12R $BaFeO_{3-x}$, let us first examine an imaginary intermediate, $Ba_8M_8O_{22}$ ($BaMO_{2.75}$) whose structure can be derived from the ideal 12R $BaMO_3$. This could be achieved by removing one oxygen from every $\frac{2}{8}$ of the BaO_3 layers in 12R $BaMO_3$ ($\frac{1}{3} \times \frac{2}{8} = \frac{2}{24}$) in such a way that the basic stacking sequence would remain intact and the symmetry center would be retained. This would require the doubling of the number of stacking layers, for example, from $(chhc)$ to $(chhc)$ $(c'hhc')$, or $(hcc'hhc'ch)$, where c' would be the new BaO_2 layer. Such a conversion would only involve a minor change in structure, namely the reorganization of oxygens in the c' layers. The product would be the 24R structure shown in Fig. 4b. The change of c to c' layers would lead to the breaking of shared corners in the c' layers, and the conversion of these corner-shared octahedra to tetrahedra. However, the 24R $Ba_8M_8O_{22}$ structure would require that some tetrahedra share faces with the octahedra centered at $(0, 0, \frac{1}{2})$ and its equivalent positions. Such a structure would be expected to be highly unstable because of the bond angle stress and electrostatic repulsion in the face-shared tetrahedra. Thus a more stable compound would form by eliminating the V atom at $(0, 0, \frac{1}{2})$ and leaving the O_6 octahedral site unoccupied,

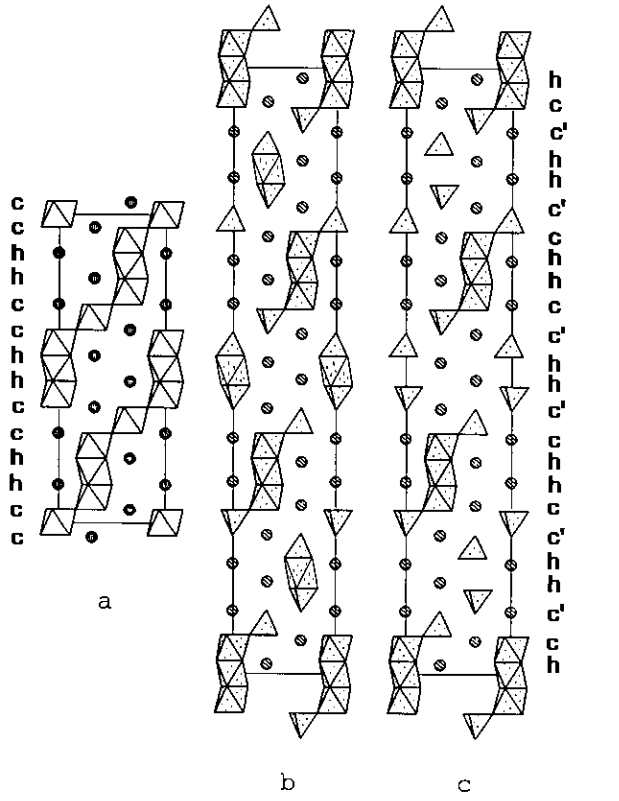

FIG. 4. Comparison of the 12R and 24R structures. Shown here are the atoms on the (1 1 0) plane and the VO_4 tetrahedra and VO_6 octahedra of the V atoms on (1 1 0). Shaded circles are Ba^{2+} ions. (a) Ideal 12R $BaMO_3$; (b) imaginary intermediate 24R $Ba_8M_8O_{22}$; (c) observed 24R $Ba_8V_7O_{22}$.

TABLE 7
Comparison of Positional Parameters for Ideal 12*R* $BaMO_3$ ($R\bar{3}m$) with Observed Values for 12*R* $BaFeO_{2.93}$

Ideal 12*R* $BaMO_3$			Observed $BaFeO_{2.93}$ (12)			
Space group: $R\bar{3}m$			$R3m$			Transformed
Atom	Site	(x, y, z)	Atom	Site	(x, y, z)	$(x, y, z + \frac{1}{24})$
Ba(1)	6*c*	$(0, 0, \frac{3}{24} \approx 0.1250)$	Ba(2)′	3*a*	$(0, 0, 0.8353)^a$	(0, 0, 0.1270)
			Ba(4)′	3*a*	(0, 0, 0.5854)	(0, 0, 0.8771)
Ba(2)	6*c*	$(0, 0, \frac{7}{24} \approx 0.2917)$	Ba(1)′	3*a*	(0, 0, 0)	(0, 0, 0.2917)
			Ba(3)′	3*a*	(0, 0, 0.4259)	(0, 0, 0.7176)
M(1)	3*a*	(0, 0, 0)	Fe(4)	3*a*	(0, 0, 0.710)	(0, 0, 0.002)
M(2)	6*c*	$(0, 0, \frac{10}{24} \approx 0.4167)$	Fe(1)	3*a*	(0, 0, 0.123)	(0, 0, 0.415)
			Fe(3)	3*a*	(0, 0, 0.310)	(0, 0, 0.602)
M(3)	3*b*	$(0, 0, \frac{1}{2} \approx 0.5000)$	Fe(2)	3*a*	(0, 0, 0.207)	(0, 0, 0.499)
O(1)	18*h*	$(-\frac{1}{6}, \frac{1}{6}, \frac{13}{24} \approx 0.5417)$	O(4)′	9*b*	(−0.178, 0.178, 0.263)	(−0.178, 0.178, 0.555)
			O(2)′	9*b*	(0.178, −0.178, 0.176)	(0.178, −0.178, 0.468)
O(2)	18*h*	$(\frac{1}{6}, -\frac{1}{6}, \frac{1}{24} \approx 0.0417)$	O(1)′	9*b*	(0.178, −0.178, 0.337)	(0.178, −0.178, 0.629)
	or	$(\frac{1}{6}, -\frac{1}{6}, \frac{15}{24} \approx 0.6250)$	O(3)′	9*b*	(−0.178, 0.178, 0.090)	(−0.178, 0.178, 0.382)

[a] The original z value of 0.8936(8) in Table 3 was apparently a typographical error. The value 0.8353 ($\sim\frac{5}{6}$) from Table 1 is more reasonable, and thus quoted here.

leading to the $Ba_8V_7O_{22}$ composition and the observed structure shown in 4c.

The above analysis, however, does not exclude the possibility of the formation of a stable 12*R* $BaVO_{3-x}$ similar to $BaFeO_{2.93}$, where the small number of oxygen vacancies are probably disordered (12) and thus there does not exist a tetrahedral FeO_4 coordination. Chamberland and Danielson (13) had reported the possible existence of a 12*R* $BaVO_3$ or $BaVO_{3-x}$ based on limited powder X-ray diffraction data. It was observed as a mixture with the 14*H* $BaVO_{3-x}$ phase synthesized at 1200°C and under high pressures (60–65 kbars), and had a significantly smaller unit cell (hexagonal a = 5.726(1) Å, c = 27.821(6) Å and V = 790.1 Å^3) than that of $Ba_8V_7O_{22}$ calculated on the same 12*R* basis (see above). Further investigations, especially under high-pressure conditions, are necessary to establish the chemical composition and true structure of the presumably 12R $BaVO_{3-x}$.

Stacking Sequence of 24R $Ba_8Ru_3Ta_2O_{18}Br_2$

Wilkens and Müller-Buschbaum (14) recently reported another 24-layer compound, the oxybromide $Ba_8Ru_3Ta_2O_{18}Br_2$. Though it has the same number of layers as $Ba_8V_7O_{22}$, its structure is significantly different from the 24R $Ba_8V_7O_{22}$ described above. All the transition metals (M = Ru and Ta) in $Ba_8Ru_3Ta_2O_{18}Br_2$ are octahedrally coordinated, and it lacks the face-shared M_3O_{12} trimers found in $Ba_8V_7O_{22}$. To compare with the 24*R* $Ba_8V_7O_{22}$ structure, we redraw the $Ba_8Ru_3Ta_2O_{18}Br_2$ structure by analogy with Fig. 4 and examine its layer stacking sequence as shown in Fig. 6. It can be described as a $(chhh'h'hhc)_3$ type stacking where c and h are BaO_3 layers and h' is a BaBr pseudolayer (Fig. 5c), still termed as

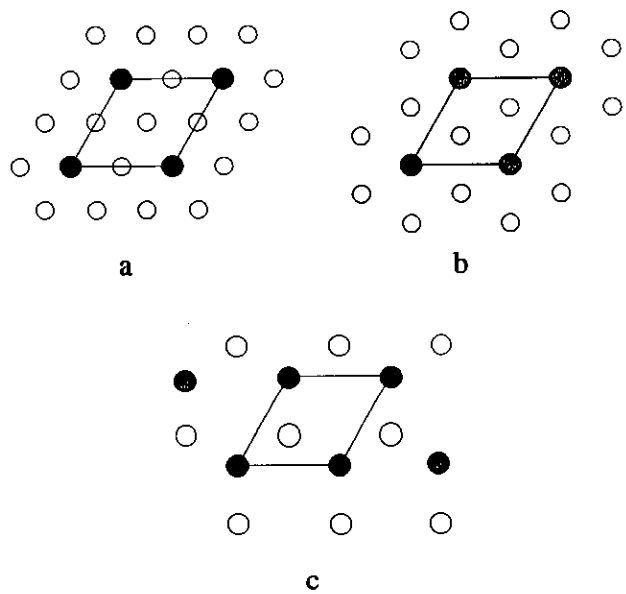

FIG. 5. Three types of Ba/O or Ba/Br layers. (a) hexagonally close-packed BaO_3; (b) hexagonally close-packed BaO_2; (c) a BaBr layer consisting of interpenetrating hexagonal Ba^{2+} and Br^- layers. Solid circles are Ba^{2+}, open circles O^{2-} or Br^-.

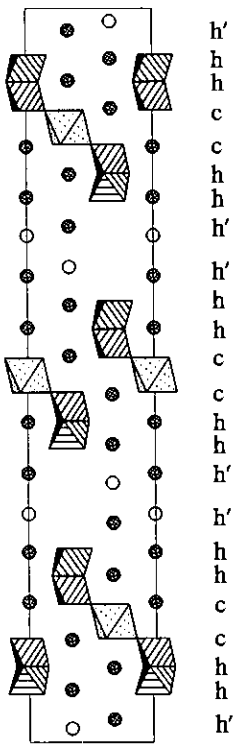

FIG. 6. The stacking sequence of 24R $Ba_8Ru_3Ta_2O_{18}Br_2$. Shown here are the atoms on the (1 1 0) plane and (Ru, Ta)O_6 octahedra of the metals on (1 1 0). Shaded circles are Ba^{2+} ions, open circles Br^- ions.

hexagonal because of its Ba position). Apparently the oxybromide has a distinctively different stacking sequence from 24*R* $Ba_8V_7O_{22}$. In addition, unlike in pure oxides, the transition metals in $Ba_8Ru_3Ta_2O_{18}Br_2$ have little direct interaction with the halide Br^- ions in the *h'* layers. Therefore the MO_6 octahedra are separated by two BaBr layers. Based on this analysis the formula can also be written as $(BaBr)_2(Ba_6Ru_3Ta_2O_{18})$, where only the second part can be described in conventional terms of stacking of close-packed Ba/O layers and space filling of transition metals.

2. Magnetic and Electrical Properties

The resistivity data for sintered pellets of $Ba_8V_7O_{22}$ are plotted in Fig. 7. Clearly, this sample is semiconducting in the investigated temperature range (145 to 295 K). The room temperature resistivity is about 12 $\Omega \cdot$ cm and there appear to be three activation energies, E_g = 0.31 eV in the temperature range from 145 to 190K, 0.36 eV from 190 to 265K, and 0.48 eV from 265 to 295 K. Electrical properties of the crystals were not investigated due to their very small size. As mentioned above the sintered pellets must contain a small amount of a reduced vanadium oxide, probably V_2O_3, so a detailed analysis of the electrical results is unwarranted.

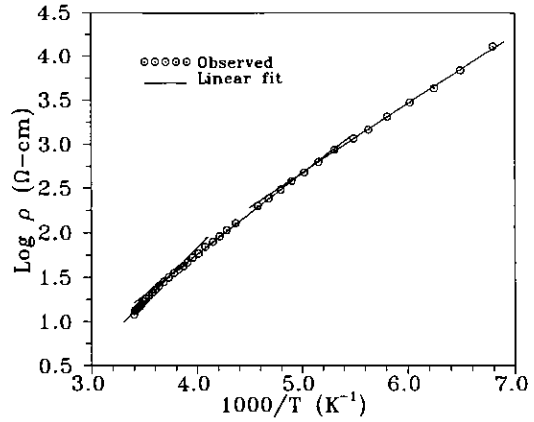

FIG. 7. Thermal variation of the electrical resistivity of a sintered polycrystalline $Ba_8V_7O_{22}$ specimen in the temperature range 145–295 K.

The magnetic properties of $Ba_8V_7O_{22}$ are shown in Fig. 8 for the polycrystalline sample and Fig. 9 for the single crystals. As has been discussed above, neither sample is phase pure. From the figures the magnetic susceptibilities do not show a simple temperature dependence as might be expected from the complexity of the crystal structure and the presence of both V^{4+} and V^{3+} in various coordination environments and connectivities. The magnetization curves of polycrystalline $Ba_8V_7O_{22}$ are shown in Fig. 10.

As the single crystal sample is contaminated only by a small amount of, presumably, diamagnetic impurity $Ba_3V_2O_8$ the results of Figs. 9 and 11 give the most reliable indication of the true magnetic properties of $Ba_8V_7O_{22}$. First, there is a weak maximum in the molar susceptibility at about 280 K followed by a significant increase beginning below 200 K. There is a clear anomaly at about 50 K and a sharp increase at 20 K. The data of Fig. 11 indicate a field

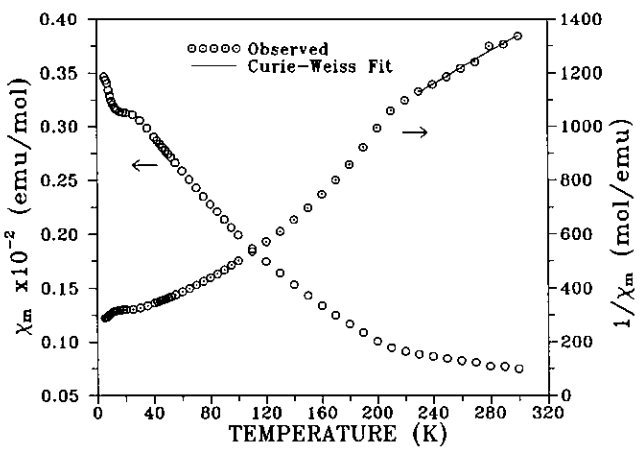

FIG. 8. Temperature dependencies of the magnetic susceptibility (per mole "$BaVO_{2.97}$") and inverse susceptibility of polycrystalline $Ba_8V_7O_{22}$ specimens.

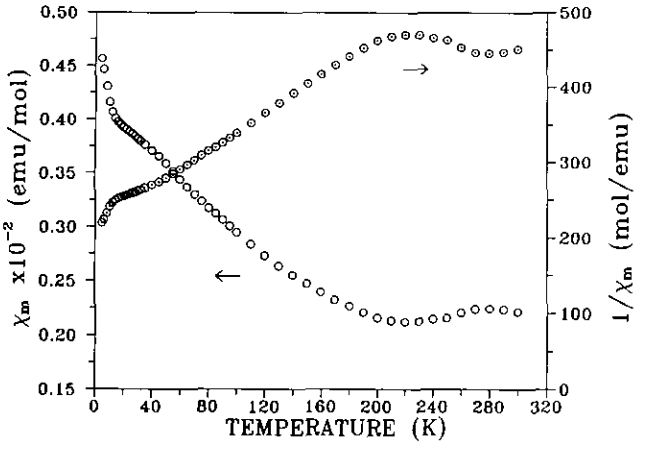

FIG. 9. Temperature dependencies of the magnetic susceptibility (per mole "$BaVO_3$") and inverse susceptibility of $Ba_8V_7O_{22}$ crystals.

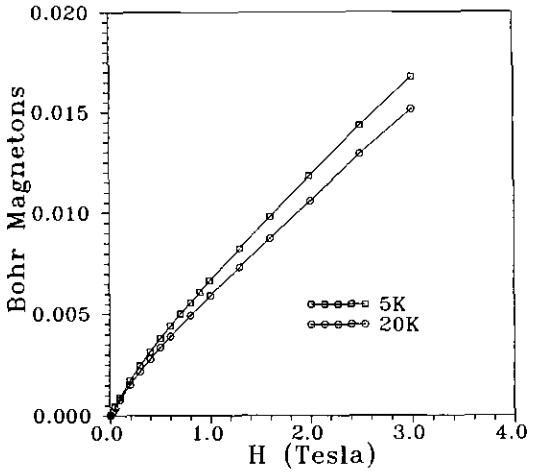

FIG. 11. Magnetization curves of $Ba_8V_7O_{22}$ crystals at 5 and 20 K.

dependent susceptibility below 20 K but no significant hysteresis. The results for the polycrystalline sample are roughly the same except that the weak maximum at 280 K is suppressed.

In the absence of information from a microscopic probe such as neutron diffraction it is very difficult to present a detailed interpretation of this very complex magnetic behavior. It does seem that the weak maximum at 280 K is a signal of short range order, which is consistent, broadly, with the layered nature of the crystal structure. Short range correlations might also be expected from the $V_3O_{12}^{14-}$ trimer unit but it seems unlikely that this unit could have ever a singlet ground state so a susceptibility maximum would not be expected. The only conclusion which can be made with confidence is that magnetic exchange interactions in this material are important up to at least room temperature.

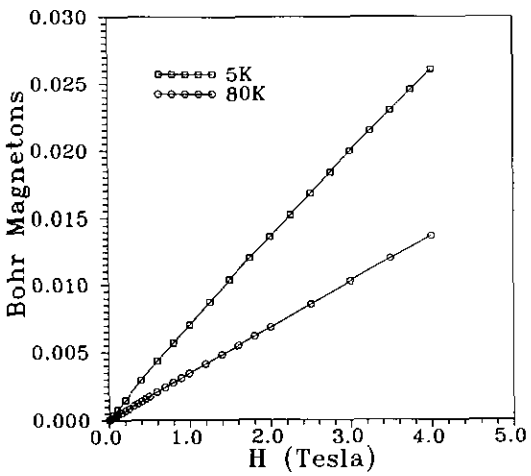

FIG. 10. Magnetization curves of polycrystalline $Ba_8V_7O_{22}$ specimens at 5 and 80 K.

ACKNOWLEDGMENTS

We thank Dr. J. Britten for collecting the single crystal X-ray diffraction data and Dr. J. Barbier for assistance with the electron microscopy work. The financial support of the Natural Science and Engineering Research Council of Canada and the Ontario Centre for Materials Research are acknowledged gratefully.

REFERENCES

1. W. Gong, J. E. Greedan, G. Liu, and M. Bjorgvinsson, *J. Solid State Chem.* **95,** 213 (1991).
2. P. W. J. Jansen, U. Spitsbergen, and P. M. De Wolff, *Recl. Trav. Chim.* **84,** 821 (1965).
3. G. Liu and J. E. Greedan, *J. Solid State Chem.* **103,** 228 (1993).
4. A. Feltz and S. Schmalfuss, *Z. Anorg. Allg. Chem.* **417,** 130 (1975).
5. T. Palanisamy, J. Gopalakrishnan, and M. V. C. Sastri, *Z. Anorg. Allg. Chem.* **415,** 275 (1975).
6. R. D. Shannon, *Acta Crystallogr. Sect. A* **32,** 751 (1976).
7. J. M. Longo and P. M. Raccah, *J. Solid State Chem.* **6,** 526 (1973).
8. M. J. Rey, Ph. Dehaudt, J. C. Joubert, B. Lambert-Andron, M. Cyrot, and F. Cyrot-Lackmann, *J. Solid State Chem.* **86,** 101 (1990).
9. B. M. Gatehouse, L. W. Guddat, and R. S. Roth, *J. Solid State Chem.* **71,** 390 (1987).
10. I. D. Brown and D. Altermatt, *Acta Crystallogr. Sect. B* **41,** 244 (1985).
11. M. Zanne and C. Gleitzer, *Bull. Soc. Chim. Fr.* **5,** 1567 (1971).
12. M. Parras, M. Vallet-Regi, J. M. Gonzalez-Calbet, J. C. Grenier, P. Hagenmuller, and J. Rodriguez-Carvajal, *Eur. J. Solid State Inorg. Chem.* **26,** 299 (1989).
13. B. L. Chamberland and P. S. Danielson, *J. Solid State Chem.* **3,** 243 (1971).
14. J. Wilkens and Hk. Müller-Buschbaum, *J. Alloys Comp.* **182,** 265 (1992).